# A New Three-Dimensional Equivalent Circuit of Diagonal Type MHD Generator

AUTHOR(S):

YOSHIDA, Masaharu; KOMAYA, Kiyotoshi; UMOTO, Juro

# A New Three-Dimensional Equivalent Circuit of Diagonal Type MHD Generator

By

Masaharu YOSHIDA*, Kiyotoshi KOMAYA* and Juro UMOTO*

(Received December 25, 1978)

**Abstract**

For a large scale diagonal type generator with oil combustion gas plasma, a new three-dimensional equivalent circuit is proposed, in which there are considered the leakage resistance of the duct insulator surface, the boundary layer, the ion slip, the effect of the finite electrode segmentation etc. Next, through the relation between the Hall voltage per one electrode pitch region and the load current obtained by use of the equivalent circuit, a suitable size and number of the space elements per region are determined. Further, by comparing in detail the electrical performances of two types of the diagonal generators with diagonal conducting and insulating sidewalls, three-dimensional effects of the sidewalls are discussed.

## 1. Introduction

Hitherto, the whole performance characteristics of MHD generators have been numerically analysed conventionally by a quasi one-dimensional theory or recently by a two-dimensional theory. However, three-dimensional phenomena occuring near the sidewall, in the duct end etc. have considerable influence on the generator characteristics.[2)3)] Lately, a new numerical claculation, to which the finite element method is applied first,[4)] has at last made the net three-dimensional analysis of local electrical performances of the generator possible. But still, it is impossible to analyse three-dimensionally the whole performance characteristics even by the above new calculation, because too many subdivision numbers of the duct are needed for a digital computer to calculate them accurately.

Now, the authors already have succeeded in analysing two-dimensionally the whole characteristics of a diagonal type generator by their new equivalent circuit method, which is suitable for analysing those, since it doesn't need so many numbers of space

* Department of Electrical Engineering

elements.[5)6)] However, as mentioned above, in the generator duct there arise three-dimensional phenomena which can't be neglected.

Accordingly, this paper first proposes a new suitable three-dimensional equivalent circuit for a large scale diagonal type generator with oil combustion gas plasma, which is an expansion of the above two-dimensional one.[7)] In the circuit there are considered the leakage resistance of the duct insulator surface, the boundary layer, the ion slip, the effect of the finite electrode segmentation etc. Next, by plotting the relation between the Hall voltage per one electrode pitch region and the load current calculated by the equivalent circuit, space elements per region are determined. Furthermore, comparing in detail the electrical performances of two types of the diagonal generators with diagonal conducting sidewalls (DCW) and insulating sidewalls (ISW), three-dimensional effects of the sidewalls, etc. are discussed.

## 2. Derivation of Three-Dimensional Equivalent Network of Diagonal Type Generator

### 2.1 Basic Equations

As the basic equations for the working gas plasma in the MHD duct, we use the following Maxwell equations

$$\nabla \times \boldsymbol{E}=0, \tag{1}$$

$$\nabla \cdot \boldsymbol{J}=0. \tag{2}$$

and the generalized Ohm law

$$\boldsymbol{J}=\sigma(\boldsymbol{E}+\boldsymbol{u}\times\boldsymbol{B})-\frac{\beta}{B}(\boldsymbol{J}\times\boldsymbol{B})+\frac{\beta\beta_i}{B^2}(\boldsymbol{J}\times\boldsymbol{B})\times\boldsymbol{B}. \tag{3}$$

In these equations, $\boldsymbol{B}$, $\boldsymbol{E}$, $\boldsymbol{J}$ and $\boldsymbol{u}$ are the applied magnetic flux density, the elctric field intensity, the current density and the gas velocity vectors, respectivey. $\beta$ and $\beta_i$ are the

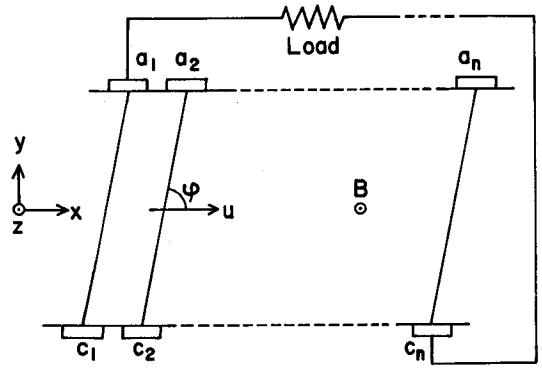


Fig. 1. Schema of diagonal type generator.

Hall parameters for electron and ion, respectively, and $\sigma$ is the electrical conductivity of the gas plasma. In addition, the secondary magnetic field induced by $\boldsymbol{J}$ is assumed to be negligible compared with $\boldsymbol{B}$, since the magnetic Reynolds number of the gas plasma is much smaller than unity under the operating conditions of our MHD generator.

Figure 1 shows a schematic diagram of the diagonal type MHD generator duct, of which one electrode pitch region in the central part is adopted as the research object of this paper. In the figure, $\varphi$ is the diagonal angle, and let us assume $\boldsymbol{B}$, $\boldsymbol{E}$, $\boldsymbol{J}$ and $\boldsymbol{u}$ as follows:

$$\begin{aligned} &\boldsymbol{B}=(0,\ 0,\ B),\\ &\boldsymbol{E}=(E_x,\ E_y,\ E_z),\\ &\boldsymbol{J}=(J_x, J_y, J_z),\\ &\boldsymbol{u}=(u,\ 0,\ 0), \end{aligned} \tag{4}$$

where $B$ is assumed constant.

Further, it is assumed that the electric quantities vary periodically with one electrode pitch $s$ along the gas flow, since such periodicity of the quantities is approximately realized in the central part of the duct. In this connection, the periodicity conditions for $\boldsymbol{E}$, $\boldsymbol{J}$ and the electric potential $\Phi$ are given by

$$\boldsymbol{E}(x+s, y, z)=\boldsymbol{E}(x, y, z), \tag{5}$$

$$\boldsymbol{J}(x+s, y, z)=\boldsymbol{J}(x, y, z), \tag{6}$$

$$\Phi(x+s, y, z)=\Phi(x, uy, z)+\Delta\Phi, \tag{7}$$

respectively, where $\Delta\Phi$ is an increment of the Hall potential per $s$.

Also in the duct, it is assumed that the pressure $p$ is kept constant, and that the gas velocity $u$ and the temperature $T$ are uniform in the gas core region and vary in the $y$ and $z$ directions according to the following turbulent profile expressions

$$\frac{u}{u_\infty}=\frac{T-T_w}{T_\infty-T_w}=\left(\frac{y}{\delta}\right)^m\left(\frac{z}{\delta}\right)^n \tag{8}$$

etc., in the boundary layers. In these equations, $\delta$ is the boundary layer thickness, $T_w$ the wall temperature, $u_\infty$ and $T_\infty$ the gas velocity and temperature, respectively, in the gas core region, with $m$ and $n$ being the constants. In addition, when $T=T_\infty=T_w$, it is assumed that only the velocity boundary layers still exist.

## 2.2 Equivalent circuit for space element

In general, the physical properties of the working gas are not uniform in the duct. Therefore, let us divide the duct space into many space elements. If each space element has a fairly small volume as compared with the one electrode pitch region, it can be assumed that the physical quantities in each element satisfy Eq. (3). Then, for each element, Eq. (3) is transformed as follows;

$$\begin{pmatrix} E_x \\ E_y - uB \\ E_z \end{pmatrix} = \frac{1}{\sigma} \begin{pmatrix} 1+\beta\beta_i & \beta & 0 \\ -\beta & 1+\beta\beta_i & 0 \\ 0 & 0 & 1 \end{pmatrix} \begin{pmatrix} J_x \\ J_y \\ J_z \end{pmatrix}. \tag{9}$$

Now, Fig. 2(a) shows one space element, where $d_e$, $s_e$ and $h_e$ are the width, length and height of the element, respectively. To simplify the analysis, let us introduce new oblique coordinates ($\xi$, $\eta$, $\zeta$) as shown in Fig. 2(b) for one space element ($d_e \times s_e \times h_e$) given in (a). The voltages $V_\xi$ , $V_\eta$ and $V_\zeta$ in the $\xi$, $\eta$ and $\zeta$ directions, respectively, between both end surfaces of the element which face each other, are given by the following relation

$$\begin{pmatrix} V_\xi \\ V_\eta \\ V_\zeta \end{pmatrix} = -\begin{pmatrix} s_e & 0 & 0 \\ h_e \cot\varphi & h_e & 0 \\ 0 & 0 & d_e \end{pmatrix} \begin{pmatrix} E_x \\ E_y \\ E_z \end{pmatrix}. \tag{10}$$

Also, the current components $I_\xi$, $I_\eta$ and $I_\zeta$ in the $\xi$, $\eta$ and $\zeta$ directions, respectively, in the element are obtained as follows.

$$\begin{pmatrix} I_\xi \\ I_\eta \\ I_\zeta \end{pmatrix} = \begin{pmatrix} d_e h_e & 0 & 0 \\ 0 & d_e s_e \sin\varphi & 0 \\ 0 & 0 & s_e h_e \end{pmatrix} \begin{pmatrix} J_\xi \\ J_\eta \\ J_\zeta \end{pmatrix}, \tag{11}$$

where

$$\begin{pmatrix} J_\xi \\ J_\eta \\ J_\zeta \end{pmatrix} = \begin{pmatrix} 1 & \cos\varphi & 0 \\ 0 & \sin\varphi & 0 \\ 0 & 0 & 1 \end{pmatrix}^{-1} \begin{pmatrix} J_x \\ J_y \\ J_z \end{pmatrix}. \tag{12}$$

Substituting Eqs. (10), (11) and (12) into Eq. (9), we get

$$-\begin{pmatrix} I_\xi \\ I_\eta \\ I_\zeta \end{pmatrix} = \begin{pmatrix} G_{11} & -G_{12} & 0 \\ G_{21} & G_{22} & 0 \\ 0 & 0 & G_{33} \end{pmatrix} \begin{pmatrix} V_\xi \\ V_\eta + e_\eta \\ V_\zeta \end{pmatrix}, \tag{13}$$

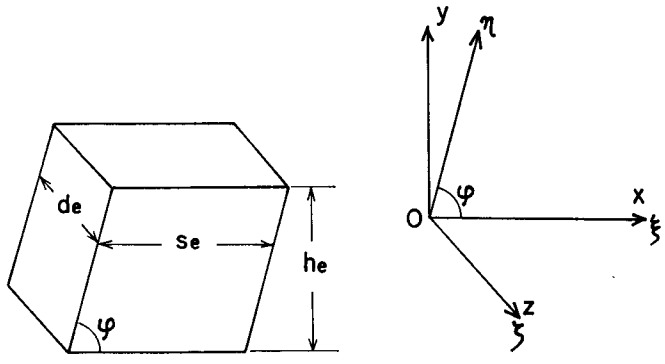


(a) (b)

Fig. 2. Space element and coordinates.
(a) Space element. (b) Coordinates.

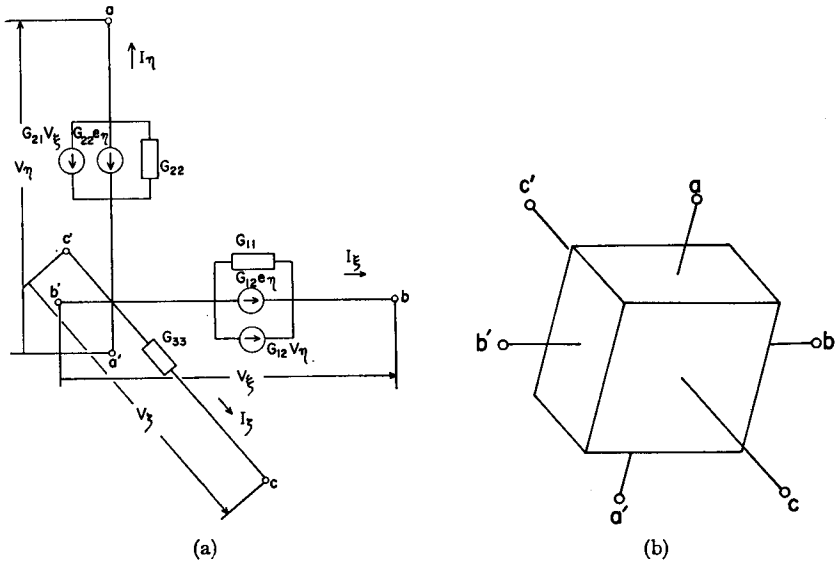


Fig. 3. Equivalent six-terminal circuit for space element.
(a) Equivalent six-terminal circuit. (b) Simplified illustration of (a).

where

$$
\begin{aligned}
G_{11} &= (1+\beta\beta_i)\mathrm{cosec}^2\varphi d_e h_e D/s_e, \\
G_{12} &= \{\beta+(1+\beta\beta_i)\cot\varphi\} d_e D, \\
G_{21} &= \{\beta-(1+\beta\beta_i)\cot\varphi\} d_e D, \\
G_{22} &= (1+\beta\beta_i) d_e h_e D/s_e, \\
G_{33} &= \sigma h_e s_e/d_e, \\
e_\eta &= h_e u B,
\end{aligned}
\tag{14}
$$

in which

$$
D=\frac{\sigma}{\beta^2+(1+\beta\beta_i)^2}.
$$

From Eqs. (13) and (14), for the one space element in Fig. 2(a) an equivalent six-terminal circuit is derived as shown in Fig. 3(a). In addition, Fig. 3(b) is a simplified illustration of the equivalent circuit in (a).

Further, for the space elements in the boundary layers in which $u$ and $T$, accordingly $\sigma$ and $\beta$, vary very steeply in the $y$ and $z$ directions, averaged expressions of Ohm's law are used, referring to Ref. (8).

### 2.3 Application of equivalent circuit to diagonal type generator

Replacing each space element by the equivalent circuit in Figs. 3, we can express one electrode pitch region of the generator in Fig. 1, for example, by an equivalent network as shown in Fig. 4, where in Figs. 1 and 4 a cross section perpendicular to the

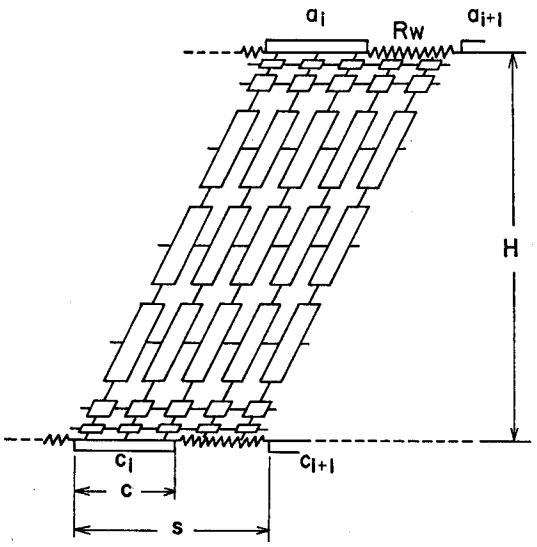


Fig. 4. Equivalent network of diagonal type generator.

gas flow and the equivalent network corresponding to it are omitted for saving space. In Fig. 4, $c$ and $H$ are the electrode width and the duct height, respectively. As seen from Fig. 4, one electrode pitch region is divided diagonally into 5 columns, 3 with the electrodes and and 2 with the insulating spacers, and between the anode and cathode the duct space by planes perpendicular to the $y$ axis into 7 layers, 3 in the gas core and 2 each in the upper and lower boundary layers. In this connection, though not illustrated, between both sidewalls the space is divided by planes perpendicular to the $z$ axis into 8 layers, 4 in the gas core and 2 each in the boundary layers of both sides. Accordingly, the number $N_s$ of space element per one electrode pitch region in Fig. 4 is 280, where only one half of the $\eta$-$z$ or $\eta$-$\zeta$ cross section and therefore $N_s/2=140$ elements are used for numerical calculation, considering symmetry.

By solving numerically the simultaneous circuit equations for the unknown node voltages in the network, those values are obtained. Furthermore, with those, the current density and the electric field intensity in each space element are evaluated, which satisfy Eqs. (1) and (2). In this connection, in Fig. 4 $R_w$ is the equivalent leakage resistance along the insulator surface between the adjacent electrodes. In numerical calculation, the value of $R_w$ is chosen as $10^5\Omega$, sufficiently large so as not to affect the calculation results.

## 3. Numerical Investigation

### 3.1 Numerical conditions

Numerical analyses are performed about a diagonal type generator with the numerical conditions listed in Table 1. Here, combustion products of a heavy oil and the

Table 1. Numerical Conditions.

| | | | |
|---|---|---|---|
| $H$ (m) | 1 | $p$ (atm) | 2 |
| $W$ (m) | 1 | $T_\infty$ (K) | 2500 |
| $s/H$ | 0 to 0.3 | $T_w$ (K) | 1500 to 2500 |
| $c/s$ | 0.6 | $u_\infty$ (m/s) | 800 |
| $\delta/H$ | 0 to 0.2 | $B$ (T) | 6 |
| $\varphi$ | 30° to 90° | $m, n$ | 1/7 |
| | | $\kappa$ | 0.5 |

oxygen of a stoichiometric factor 1.1 is used as the working gas, where KOH and $K_2SO_4$ are seeded so that the potasium is contained in the ratio of 1 wt% to the combustion gas. In this Table 1, $w$ and $\kappa$ are the duct width and the loading factor, respectively, where $\beta_i$ is assumed as zero, since the ion slip effect is very small.

Next, Reference 1 gives the gas tables of the above working gas. From the table, the dependences of $\sigma$ and $\beta$ on $B, p$ and $T$ have been determined as follows;

$$\left.\begin{aligned}\sigma&=89.9p^{-0.510}T^{1.055}\exp(-25190/T),\\ \beta&=4.43\times10^{-4}p^{-0.990}T^{0.970}B.\end{aligned}\right\} \tag{15}$$

### 3.2 Number and Size of Space Element

Figure 5 shows the $V_X$-$I_L$ characteristic curves of the DCW and the ISW generators for $s/H=\delta/H=0.1$, $\varphi=45°$ and $T_w=1500$ K, where $V_X$ and $I_L$ are the Hall voltage per $s$

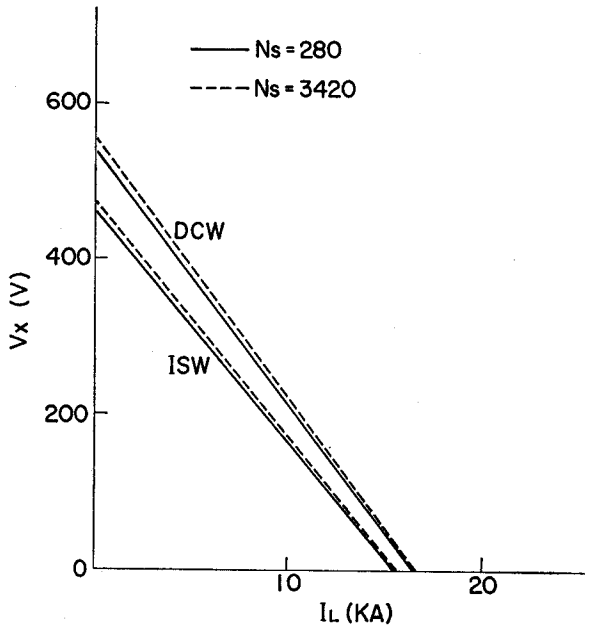


Fig. 5. $V_X$-$I_L$ characteristic curves when $s/H=\delta/H=0.1$, $\varphi=45°$ and $T_w=1500$ K.

and the load current, respectively. In the figure, the solid lines show the calculation results obtained with the equivalent network in Fig. 4, which has $N_s=280$. The dotted lines indicate the results obtained with the equivalent network of $N_s=3420$, where one electrode pitch region is divided idagonally into 10 columns, 6 with the electrodes and 4 with the insulating spacers. Between the anode and cathode, the duct space is divided by planes perpendicular to the $y$ axis into 19 layers, 9 in the gas core and 5 each in the upper and lower boundary layers. Further, between both sidewalls, the space is divided by planes perpendicular to the $z$ axis into 18 layers, 8 in the gas core and 5 each in both boundary layers on both sides. In Fig. 5, both the solid and dotted lines agree well. Accordingly, it is seen that the equivalent network in Fig. 4 will give good approximate values of the power density $P$, the electrical efficiency $\eta_e$ etc. of the generator. In the next section, the calculation results plotted in Figs. 6 to 9 were obtained with the equivalent network of $N_s=280$, and those in Figs. 10 and 11 with the equvalent network of $N_s=3420$. In this connection, it was ascertained that we can't obtain good calculation results when there are fewer $N_s$ than in Fig. 4 and accordingly, space elements of larger sizes are used for calculation.

### 3.3 Comparison of DCW and ISW Generators

Figure 6 shows the influence of $T_w$ on $P$ and $\eta_e$ of the DCW and ISW generators, where $s/H=\delta/H=0.1$, $c/s=0.6$ and $\varphi=45°$. Also in Fig. 6, the two-dimensional cal-

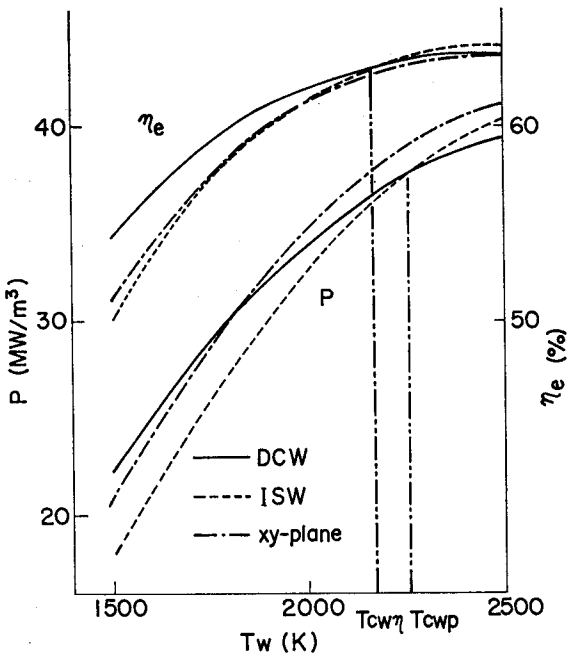


Fig. 6. Influence of $T_w$ on $P$ and $\eta_e$ when $s/H=\delta/H=0.1$ and $\varphi=45°$.

culation results in $x$–$y$ plane are shown.

The figure shows that the existence of the boundary layer near the sidewall reduces $P$ of the ISW generator, and it is considerably lower than $P$ by the two-dimensional analysis. $P$ and $\eta_e$ of the ISW generator decrease as $T_w$ decreases. However, the decrease of $P$ and $\eta_e$ in DCW generator with the decrease of $T_w$ is fairly low, compared with that in the ISW generator. $P$-$T_w$ and $\eta_e$-$T_w$ characteristic curves of the DCW and the ISW generators intersect at temperatures $T_{cwp}$ and $T_{cw\eta}$, respectively, which let us call the critical wall temperatures for $P$ and $\eta_e$, respectively. In other words, in the case of the hot duct wall of $T_w > T_{cwp}$, the ISW generator has better characteristics than the DCW generator, but in the case of the cold wall of $T_w < T_{cwp}$ the oposite result appears. Next, for the same numerical conditions as in Fig. 6, except

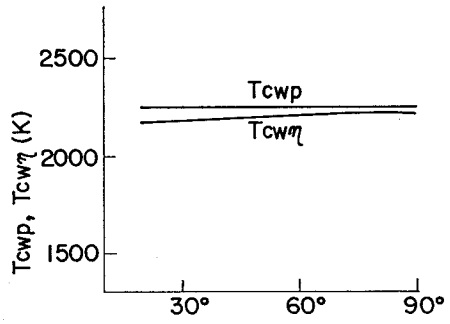


Fig. 7. Influence of $\varphi$ on $T_{awp}$ and $T_{cw\eta}$ when $s/H=\delta/H=0.1$.

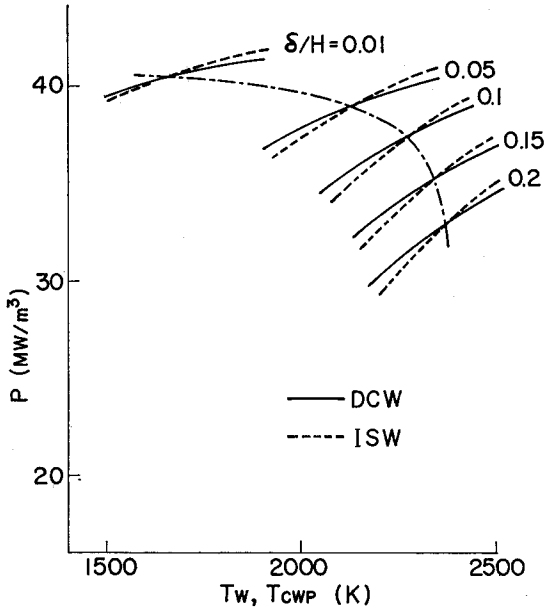


Fig. 8. Influence of $\delta/H$ on $P$ and $T_{cwp}$ when $s/H=0.1$ and $\varphi=45°$.

$\varphi$, the variations of $T_{cw\phi}$ and $T_{cw\eta}$ with $\varphi$ are plotted in Fig. 7, from which it is seen that they depend little on $\varphi$.

Figure 8 shows the influence of $T_w$ and $\delta/H$ on $P$ of the DCW and the ISW generators for the same numerical conditions as in Fig. 6, except $\delta/H$. The figure indicates that $P$ decreases and $T_{cw\phi}$ increases with $\delta/H$. From the above mentioned results, we see that the influence of the sidewall structure on $P$ is very important. Let us investigate it further.

The MHD generator performance is deteriorated by a circulating current which is created as a result of shorting the Hall electric field by the finitely segmented electrodes. This is called the effect of finite electrode segmentation, and it is well known that this effect increases with the value of $s/H$. Since the DCW generator has sidewall electrodes, the effect rises near the sidewalls as well as the main walls. On the other hand, since the sidewalls of the ISW generator consist of an insulating material, the effect doesn't occur near the sdewall. Therefore, it is thought that the ISW generator has better characteristics than the DCW generator, and the latter inferiority becomes large with the value of $s/H$.

Now, Fig. 9 shows the influence of $s/H$ on $P$ of the DCW and the ISW generators

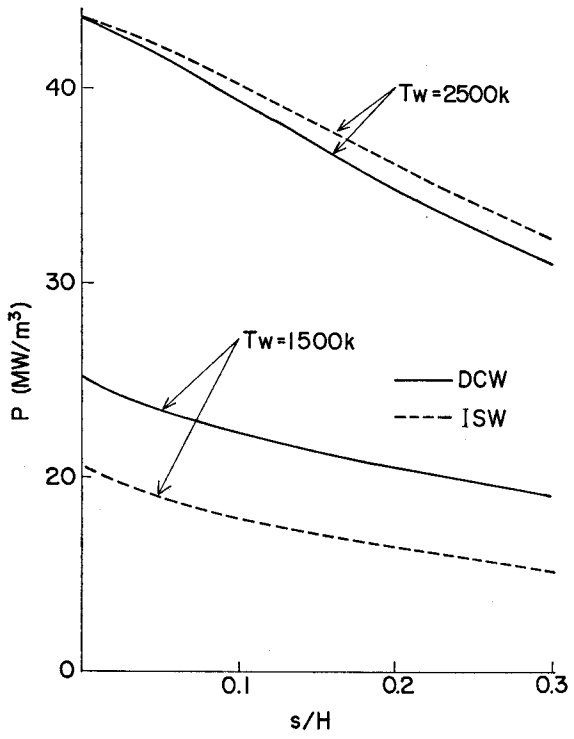


Fig. 9. Influence of $s/H$ on $P$ when $\varphi=45°$, $T_w=2500$ and 1500 K, where $\delta/H=0.1$, respectively.

when $\delta/H=0.1$, $\varphi=45°$, $T_w=2500$ and 1500 K. In the case of $T_w=2500$ K, we can see that the effect of the finite segmentation of the sidewall electrode deteriorates the characteristics of the DCW generator. However, in the case of $T_w=1500$ K, the DCW generator has better characteristics than the ISW generator. This phenomenon can't be explained with the effect of the finite segmentation of the sidewall electrode.

The current distributions at $z=\delta/2$ near a sidewall electrode of the DCW duct are shown in Figs. 10(a) and (b) for $T_w=2500$ and 1500 K, respectively, where $s/H=\delta/H=$

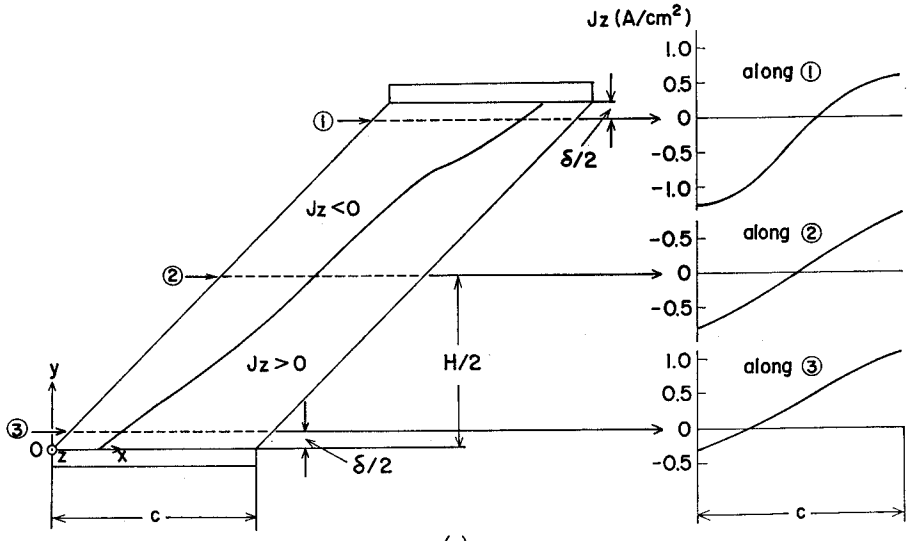


(a)

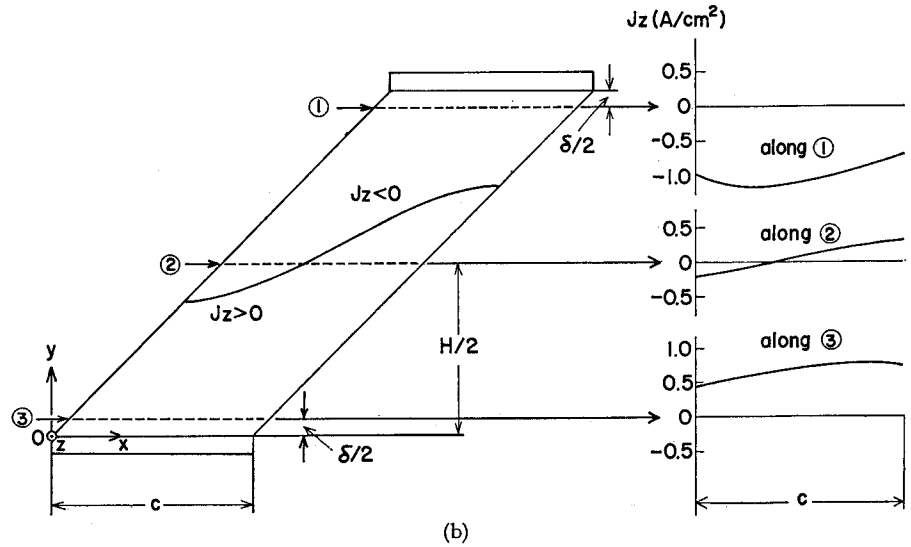


(b)

Fig. 10. Current distributions at $z=\delta/2$ near sidewall electrode of DCW generator.
(a) $T_w=2500$ K. (b) $T_w=1500$ K.

0.1 and $\varphi=45°$. In these figures, the current flows into the sidewall electrode in the domain of $J_z>0$ and flows out of it in the domain of $J_z<0$.

Fig. 10(a) for $T_w=2500$ K indicates that the current circulates near the sidewall electrode due to the effect of the finite segmentation of the sidewall electrode. On the other hand, in Fig. 10(b), for $T_w=1500$ K, the current doesn't circulate and accordingly in the DCW generator, the sidewall electrode doesn't so much deteriorate the electrical characteristics. In this connection, in the case of $T_w=1500$ K, the current density in the ISW generator becomes very small in the boundary layer, since both conductivities of the gas plasma there and the insulating sidewall are very low. Therefore, in the case of the low wall temperature, it is understood that the cahracteristics of the ISW generator become somewhat worse than those of the DCW generator. Finally, Figs. 11(a) and (b) show the distributions of $J_y$ in the $x$-$z$ plane at $y=\delta/1000$, $z=\delta/2$ and at $y=\delta/1000$, $z=w/2$, respectively, in the DCW duct, where $s/H=\delta/H=0.1$, $\varphi=45°$, $T_w=2500$ and 1500 K. From these figures, it is seen that the current concentrates at the upstream end of the anode due to the finite segmentation effect in the case of $T_w=2500$ K. On the other hand, in the case of $T_w=1500$ K, the current concentration is fairly relaxed and it flows pretty uniformly compared with the former case.

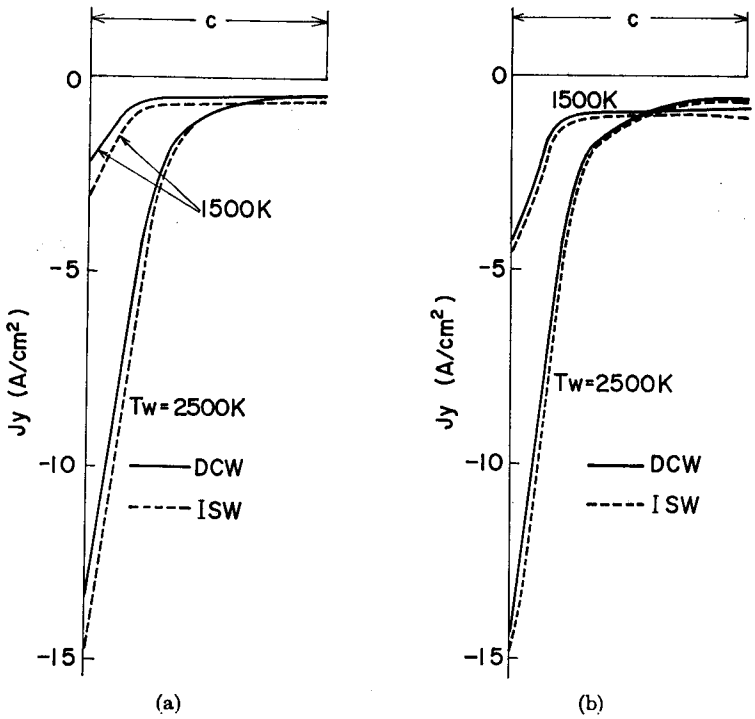


Fig. 11. Distribution of $J_y$ at $y=H-\delta/1000$ near anode of DCW generator.
(a) $z=\delta/2$. (b) $z=w/2$.

## 4. Conclusions

(1) For a diagonal type generator, a new three-dimensional equivalent circuit was proposed, in which there are considered the leagkae resistance of the duct wall surface, the boundary layer, the ion slip, the effect of finite electrode segmentation etc.

(2) To obtain the $V_X$-$I_L$ characteristic curves of the DCW and the ISW generators with satisfactory accuracy, at least one electrode pitch region should be divided diagonally into 5 columns, 3 with the electrodes and 2 with the insulating spacers. Between the anode and the cathode, the duct space should be divided by planes perpendicular to the $y$ axis into 7 layers, 3 in the gas core and 2 eadh in the upper and lower boundary layers. Further, between both sidewalls the space should be divided by planes perpendicular to the $z$ axis into 8 layers, 4 in the gas core and 2 each in the boundary layers on both sides.

(3) For $T_w > T_{cwp}$, the electrical characteristics of the DCW generator is inferior to those of the ISW generator because of the effect of the finite segmentation of the sidewall electrode. On the other hand, for $T_w < T_{cwp}$, the opposite result appears. In addition, $T_{cwp}$ and $T_{cw\eta}$ depend little on $\varphi$, but increase with $\delta/H$.

### References

1) Technical Report of the Investigation Committee of MHD Generator Plant in Japan, 1973.
2) Y. C. L. Wu and G. Rajagopal; 16th Symp EAM, VII-2 (1977).
3) J. C. Cutting, C. D. Maxwell and R. T. Ling; ibid, VII-4 (1977).
4) T. Hara and J. Umoto; 17th Symp EAM, B. 5 (1978).
5) M. Yoshida and J. Umoto; Ann. Meet. of IEE Japan, G1-32 (1978).
6) M. Yoshida and J. Umoto; THIS MEMOIRS, 39, 4, 427 (1977).
7) M. Yoshida, K. Komaya and J. Umoto; Ann. Meet. of IEE Japan G1-33 (1978).
8) R. J. Rosa; "Magnetohydrodynamic Energy Conversion." (McGraw Hill, 1968) p. 74.